J. Astrophys. Astr. (2022) 43:61
https://doi.org/10.1007/s12036-022-09846-3

System identification and tuning applied to pseudo open loop control in multi-conjugate adaptive optics

ALEXANDRE J. T. S. MELLO[1,*], ELDER OROSKI[1], VICTOR B. FRENCL[1], GUIDO AGAPITO[2] and DANIEL R. PIPA[1]

[1]Department of Electrical Engineering, Universidade Tecnológica Federal do Paraná (UTFPR), Curitiba, PR 80230-901, Brazil.
[2]Osservatorio Astrofisico di Arcetri (INAF), 50125 Firenze, Italy.
Corresponding author. E-mail: ajmello@utfpr.edu.br

MS received 6 October 2021; accepted 23 March 2022

Abstract. Pseudo open loop control is a robust control technique for use in multi-conjugated adaptive optics systems for wide-field atmospheric turbulence compensation. This control technique helps to minimize the deleterious effects of optical defects in the system. We propose to use system identification on open-loop and closed-loop and frequency response analysis to achieve a better tuning and characterization of a POLC system. Our results show that system identification can be used to determine the robustness of the system, and can also be used to obtain a model for system tuning.

Keywords. Multi conjugate adaptive optics—open-loop gain design—pseudo open loop control—system identification.

1. Introduction

Multi-conjugate adaptive optics (MCAO) (Beckers 1989) is a technique to compensate atmospheric turbulence in astronomical telescopes in a wide field of view. To expand the field of view in relation to classical adaptive optics (AO), MCAO technique uses multiple mirrors optically conjugated to corresponding turbulence layers, resulting in a multi-directional compensation and expanding the narrow corrected field of view of classical AO.

In order to measure the turbulence in a wide field of view, multiple wave front sensors (WFS) are required. Then, tomographic techniques are applied to convert these measurements, which represent the sum of turbulence in each direction, to command for the mirrors, that are optically conjugated to the turbulence layers.

If we consider the system to be linear, it is possible to apply linear algebra theorems and properties in order to obtain a tomographic matrix.

Ellerbroek & Vogel (2003) propose such a matrix that intends to minimize the mean squared phase variance associated to the residual wavefront after mirror reflections. The turbulence and noise covariance matrices are taken into account to obtain better results.

In classical AO the system can be calibrated measuring the interaction matrix of the system, and using it to obtain a control matrix, which will retain information of the system, including its optical defects. However in MCAO it is necessary to rely on tomography, and the respective tomographic matrix has limited information about any system imperfections. Gilles (2005) and Piatrou & Gilles (2005) show that the use of a tomography technique with the closed-loop control (CLC) can lead to instabilities in the presence of optical imperfections, known as misregistrations. Also, they show that the pseudo open loop control (POLC) is more robust than CLC. A POLC system includes information of the interaction function in the control system loop, which can explain the improved system stability. It is important to notice that the use of POLC in MCAO is not yet tested in the sky. Recent papers such as Basden *et al.* (2019) and Wang & Ellerbroek (2012) discuss efficient computational implementations of POLC.

Published online: 10 September 2022

Since the most efficient wavefront correction algorithms are usually model-based, the modeling accuracy of the system influences the wavefront correction performance (Sun *et al.* 2018). When a highly accurate mathematical model is required, system identification (SI) methods become very appealing. These methods are based on system data, and hence, the respective obtained mathematical model represents the system exactly as it was built. Thus, in this work, we turn to the problem of SI, control systems design and tuning methods applied to those systems. In control systems theory it can be found a wide variety of control design and tuning methods, but most of them rely on some knowledge of the system, commonly expressed as a mathematical model. In this context, the more accurate the mathematical model, the more effective the design and tuning of the system control.

SI theory is used in order to obtain information about the behavior of the system and its mathematical model (Ljung 1999). Here, we show how it can be used in two important cases. The first can be divided into two parts: (i) obtaining knowledge about the system and (ii) testing closed-loop stability with a method that could be applied in a real system. The second case is to use it for a control tuning, obtaining the open-loop model of the system. To complete this control tuning we propose to use the Fourier Transform of the measured turbulence, information which is available and can be obtained in the real system before the definitive control tuning.

The organization of the paper is as follows: Section 2 describes some SI methods; Section 3 presents the POLC and CLC techniques; Section 4 describes the main simulations carried out; Section 4.1 proposes a stability analysis based on the results obtained from the SI; Section 4.2 presents SI in the open-loop control gain design context, useful for system tuning when coupled with the frequency response of the turbulence measurement and Section 5 presents the conclusions to this work.

2. Modeling and identification

Achieving a representative mathematical model for a real system is appealing in control systems, specially for control design (Åström & Hägglund 2011); in AO, it is not different. In order to correct wavefront distortion caused by atmospheric turbulence, control actions over a deformable mirror (DM) are applied to instruments assisted by AO. If the system already has a dynamic model, it is easier to design a controller for the system (Ljung 1999).

In this context, modeling a system may provide a better understanding and prediction of its behavior in several situations. There are basically two main processes to obtain a mathematical model for a real system. First, we have the physics laws based modeling (PLBM), also known as 'white-box modeling', which is based on fundamental physics laws that can describe analytically the system dynamics. These type of models are commonly generic and they represent a large class of systems, but they are not accurate enough to represent a very specific system. Second, we have the data based modeling (DBM), also known as 'black-box modeling', which is grounded on extracting the system dynamics solely through its input and output data.

One of the fields of modern control systems, which is responsible for creating models based on empirical data, is known as system identification (SI). One can define it as a method of measuring the mathematical description of a system by processing the observed inputs and outputs of the system (Billings 2013).

Generally, a model obtained from a SI technique is more accurate in describing a specific given system than generic models that are based only on physical laws (Isermann & Munchhof 2011).

One of the main purposes of this paper is the application of SI theory, aiming to get a more accurate and more efficient dynamic model for the system, in order to carry out the control tuning. The model is developed considering only inputs and outputs data, in a DBM 'black-box' approach. In this work, we use simulated data, but when applying to an AO system, telemetry data from the real system would be used. Therefore, the MCAO system is modeled using SI, in order to improve the control tuning process.

It is important to notice that MCAO systems are inherently multiple input multiple output (MIMO) systems. However, as a modeling strategy for control purposes, it will be considered the hypothesis that a MIMO system can be simplified as a composition of several single input single output (SISO) systems, without loss of generality. This simplification is a common practice in multivariate control theory, and it is called decentralized feedback control (Skogestad & Postlethwaite 2005). For a not diagonally dominant system, like the MCAO systems, it is necessary to use a decoupling matrix, in order to consider each component of the control system separately (Åström & Hägglund 2011).

The most common method used in AO control is to use the response from each actuator in the sensor to build a matrix — the interaction matrix — and then use its inverse form — the control matrix — to multiply the

measurements before applying the controller (commonly a simple integrator). This matrix converts information from the sensor space to the actuator space. However, in the control theory point of view, the interaction matrix represents the system response at steady state, and its inverse, the control matrix, is considered a decoupling matrix because, after applying this matrix, each controller will see the system as a SISO system focused in the corresponding actuator.

A decoupled SISO system obtained from a MIMO system can be seen in Figure 1, in which a model is estimated only through its inputs $u_i(k) \in \mathbb{R}$ and its outputs $y_i(k) \in \mathbb{R}$, being $k \in \mathbb{N}$ the discrete time, and $i \in \mathbb{N}$ the index for the ith SISO system. The difference between the estimated and real outputs, $\hat{y}_i(k)$ and $y_i(k)$, respectively, are given by $e_i(k) \in \mathbb{R}$.

It is important to note that in DBM approach, only input and outputs data, $u_i(k)$ and $y_i(k)$, respectively, are used to determine (i) the structure and (ii) the parameters of the model. In Sections 2.1–2.4, some dynamic models employed in this paper, based on SI theory, are presented.

2.1 *ARX models*

Let a discrete SISO system be represented by the function $y_k = f_k(y_{k-n}, u_{k-m})$, with input $u_k \in \mathbb{R}$ and output $y_k \in \mathbb{R}$, being $k, m, n \in \mathbb{N}$ discrete-time indexes. In this context, auto regressive with eXogenous input (ARX) models are composed of linear combinations of both input and output values, as shown in Equation (1):

$$y_k = \sum_{n=1}^{M_y} a_n y_{k-n} + \sum_{m=1}^{M_u} b_m u_{k-m}, \tag{1}$$

in which $M_y, M_u \in \mathbb{N}$ are input and output regression orders and $a_n, b_m \in \mathbb{R}$ are coefficients for regressors y_k and u_k, respectively.

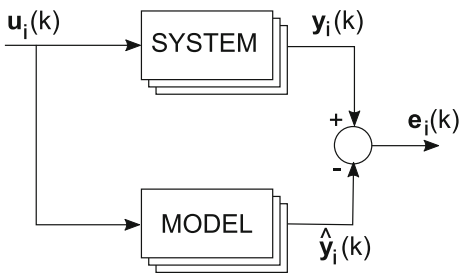

Figure 1. Block diagram example of an output error model, with an input $u_i(k)$, an output vector $y_i(k)$, an estimated output $\hat{y}_i(k)$ and an error $e_i(k)$.

Concerning computational implementation, ARX models do not require high computational effort, however they present parameters inconsistencies for most practical systems (Tufa *et al.* 2007). In order to solve this issue, nonlinear models are commonly employed. Many of nonlinear models are based on the linear ARX model with some adaptations, as follows in Section 2.2.

2.2 *Hammerstein and Wiener models*

The first and most simple notion of a nonlinear system is achieved by a cascaded connection between a linear dynamic block and some static nonlinearities (Isermann & Munchhof 2011).

The linear dynamic block can be defined in different ways, e.g., differential/difference equations, transfer functions and state space representations. In this work, it will be applied to the frequency domain version of the ARX model, i.e., the unilateral $\mathcal{Z}$-transform of y_k. The definition of the unilateral $\mathcal{Z}$-transform, for a known sequence x_k, is given by

$$\mathcal{Z}\{x_k\} = \mathcal{X}(z) = \sum_{k=0}^{\infty} x_k z^{-k}, \quad z \in \mathbb{C}. \tag{2}$$

It is important to notice that the $\mathcal{Z}$-transform of a known sequence has the same dimension of the respective sequence; e.g., if x_k has dimension n, then $\mathcal{X}(z)$ also has dimension n.

In this scenario, consider a discrete time block, with input $u_k \in \mathbb{R}$ and output $y_k \in \mathbb{R}$:

$$\mathcal{H}(z) = \frac{\mathcal{Y}(z)}{\mathcal{X}(z)} = \frac{\mathcal{Z}\{y_k\}}{\mathcal{Z}\{x_k\}}. \tag{3}$$

In the Hammerstein and Wiener models, which are illustrated in Figures 2 and 3, and considering SISO systems, the nonlinear blocks can be defined as any nonlinear functions $f_h(\cdot)$: $\mathbb{R} \to \mathbb{R}$ for the Hammerstein model, and $f_w(\cdot)$: $\mathbb{R} \to \mathbb{R}$ for the Wiener model. In the case of MIMO systems, the mappings can be generalized as $\mathbb{R}^\alpha \to \mathbb{R}^\beta$, being $\alpha, \beta \in \mathbb{N}^+$, in which $\mathbb{N}^+$ stands for the set of positive natural numbers.

In the dynamic block, the current output depends on its past values, while the output of static blocks depends only on its current inputs. The Hammerstein model structure is composed of a nonlinear static block, represented by the function $f_h(\cdot)$, followed by a linear dynamic block $H(q)$ (Pintelon & Schoukens 2012), as expressed in (4) and (5), and in Figure 2(a).

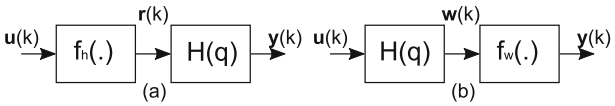

Figure 2. (a) Hammerstein model. (b) Wiener model. The functions $f_h(\cdot)$ and $f_w(\cdot)$ stand for the static nonlinearities, $H(q)$ for the linear dynamic block and q is the advance operator in discrete time.

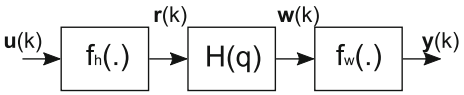

Figure 3. Hammerstein–Wiener model. $f_h(\cdot)$ stands for the input nonlinearity, $H(q)$ stands for the linear dynamic block and $f_w(\cdot)$ for the output nonlinearity.

$$r_k = f_h(u_k), \tag{4}$$

$$y_k = H(q)r_k, \tag{5}$$

in which q is the advance operator in discrete time and $r_k \in \mathbb{R}$ is an intermediate signal. Equations (4) and (5) can also be represented in a compact form, as follows:

$$y_k = H(q)f_h(u_k). \tag{6}$$

Inverting the block order, a Wiener model is obtained, as shown in (7) and (8), and in Figure 2(b).

$$w_k = H(q)u_k, \tag{7}$$

$$y_k = f_w(w_k), \tag{8}$$

in which $w_k \in \mathbb{R}$ is an intermediate signal. These equations can also be expressed in a compact form, as follows:

$$y_k = f_w(G(q)u_k). \tag{9}$$

2.3 *Hammerstein–Wiener model*

The Hammerstein–Wiener model (HWM) can be seen as a fusion of Hammerstein and Wiener models. This model is composed of one linear dynamic block, $H(q)$, positioned between two static nonlinearities, represented by the nonlinear functions $f_h(\cdot)$ and $f_w(\cdot)$ (Isermann & Munchhof 2011).

The structure of this model can be seen in Figure 3, and its mathematical form is expressed in Equations (10)–(12)

$$r_k = f_h(u_k), \tag{10}$$

$$w_k = H(q)r_k, \tag{11}$$

$$y_k = f_w(w_k), \tag{12}$$

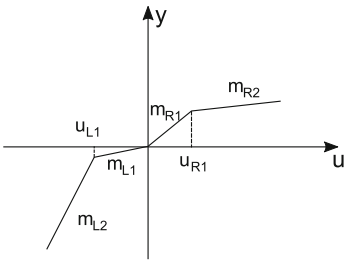

Figure 4. Example of a 'piece-wise linear' function with four (two in the 1st quadrant and two in the 3rd quadrant) segments.

or, in a compact form, as follows:

$$y_k = f_w(H(q)f_h(u_k)). \tag{13}$$

In this work, static nonlinearities applied to HWM models are 'piece-wise linear' type. For more details, see (D'Ambrosio *et al.* 2010). One of the most important nonlinearities in the HWM will be presented in Section 2.4.

2.4 *Piece-wise linear static nonlinearity*

The nonlinearity of the type 'piece-wise linear' was used in this paper in the Wiener model and the HWM. Static nonlinearities can be represented by 'piece-wise linear' functions, as shown in Equation (14). Its graphical form is depicted in Figure 4.

$$y = \begin{cases} m_{R1}u, & \text{if } 0 \le u \le u_{R1}, \\ m_{R2}(u - u_{R1}) + m_{R1}u_{R1}, & \text{if } u > u_{R1}, \\ m_{L1}u, & \text{if } u_{L1} \le u < 0, \\ m_{L2}(u - u_{L1}) + m_{L1}u_{L1}, & \text{if } u < u_{L1}, \end{cases} \tag{14}$$

in which m_{L1}, m_{L2}, m_{R1} and m_{R2} are the slopes of the linear segments, u_{L1} is a constant for negative inputs and u_{R1} is a constant for positive inputs.

It is important to mention that 'piece-wise linear' model structure is relevant for being the nonlinear part of the Hammerstein–Wiener model, which is responsible for model the overall dynamic of a MCAO system. Furthermore, these nonlinear static functions were chosen because they are one of the most common tools in nonlinear SI frameworks.

3. MCAO control

In this section we will first define the minimum-variance reconstructor (MVR), and then, we will show why it cannot be used by a simple CLC, before introducing the POLC method.

In the control theory point of view, the tomographic matrix can be seen as a decoupling matrix of a MIMO system. In MCAO control it is common to use a regularized inverse of the interaction matrix to build that matrix. However, in this work, we will focus in the use of MVR to build the tomographic matrix.

3.1 *The minimum–variance reconstructor*

This section discusses the static aspect of the control system, i.e., the reconstruction process. Next, in Section 3.2 we will deal with the dynamic part, i.e., the temporal control through the discrete-time filter.

The MVR is based on linear mapping operations involving influence matrices, such as $\mathbf{G}_a \in \mathbb{R}^{i\times\ell}$ — an influence matrix that maps the actuator control vector in the sensor vector space — and $\mathbf{G}_x \in \mathbb{R}^{i\times j}$ — an influence matrix that maps the atmospheric turbulence vector also in the sensor vector space. To represent the turbulence using a vector, it is usual to decompose the wavefront surface as a combination of indices of a basis, like the Zernike Polinomials (Noll 1976) or the Karhunen–Loève basis (Wang & Markey 1978).

The mentioned transformation in the sensor space can be represented mathematically in (15):

$$\mathbf{s}_k^{\mathrm{ol}} = \mathbf{G}_x\mathbf{x}_k + \mathbf{n}_k, \tag{15}$$

in which $\mathbf{a}_k \in \mathbb{R}^{\ell}$ is the actuator control vector, $\mathbf{s}_k^{\mathrm{ol}} \in \mathbb{R}^{i}$ is the WFS vector, or slopes vector — measuring in open-loop — $\mathbf{x}_k \in \mathbb{R}^{j}$ is the atmospheric turbulence vector, or turbulence vector and $\mathbf{n}_k \in \mathbb{R}^{i}$ is the WFS noise.

The reconstruction matrices to be obtained by the MVR are $\mathbf{E} \in \mathbb{R}^{j\times i}$, which maps the WFS vector to the turbulence vector, and $\mathbf{F} \in \mathbb{R}^{\ell\times j}$, which maps the turbulence vector to the actuator control vector. These two reconstructors are represented mathematically in the following linear mappings:

$$\mathbf{x}_k = \mathbf{E}\mathbf{s}_k^{\mathrm{ol}}, \tag{16}$$

$$\mathbf{a}_k = -\mathbf{F}\mathbf{x}_k. \tag{17}$$

The turbulence vector $\mathbf{x}_k$ can be obtained using the reconstruction matrix $\mathbf{E}$ from the measurements vector directly if the system is operating in open-loop and $\mathbf{a}_k \in \mathbb{R}^{\ell}$ is the actuator control vector. In Ellerbroek & Vogel (2003), it is shown that the reconstruction matrices $\mathbf{E}$ and $\mathbf{F}$ can be defined as functions of other important matrices, as follows:

$$\mathbf{E} = \left(\mathbf{G}_x^{\intercal}\mathbf{C}_{nn}^{-1}\mathbf{G}_x + \mathbf{C}_{xx}^{-1}\right)^{-1}\mathbf{G}_x^{\intercal}\mathbf{C}_{nn}^{-1}, \tag{18}$$

$$\mathbf{F} = \left(\mathbf{H}_a^{\intercal}\mathbf{W}\mathbf{H}_a + \gamma\mathbf{I}\right)^{-1}\mathbf{H}_a^{\intercal}\mathbf{W}\mathbf{H}_x, \tag{19}$$

in which $\gamma \in \mathbb{R}^{+}$ is a real positive constant, $\mathbf{I} \in \mathbb{R}^{\ell\times\ell}$ is an identity matrix, $\mathbf{W}$ depends on the shape of the aperture and on the influence functions used to represent the continuous turbulence, $\mathbf{C}_{xx} \in \mathbb{R}^{j\times j}$ is the turbulence covariance matrix, $\mathbf{C}_{nn} \in \mathbb{R}^{i\times i}$ is the WFS noise covariance matrix, $\mathbf{H}_a \in \mathbb{R}^{j\times\ell}$ and $\mathbf{H}_x \in \mathbb{R}^{j\times j}$ represent, via linear transformation, the action of DMs and the action of turbulence, respectively.

Matrices $\mathbf{H}_a$ and $\mathbf{H}_x$ appear in the residual phase equation as transformation matrices from the turbulence and the actuator control vector, respectively, as follows:

$$\boldsymbol{\epsilon}_k = \mathbf{H}_x\mathbf{x}_k - \mathbf{H}_a\mathbf{a}_k, \tag{20}$$

in which $\boldsymbol{\epsilon}_k \in \mathbb{R}^{j}$ is the residual phase profile vector.

3.2 *Closed-loop control with minimum-variance reconstructor*

In CLC, the WFS is measuring the residual wavefront after the correction. This means we are measuring in closed loop, with the inclusion of $\mathbf{a}_k$ as the actuator control vector, which is delayed because of the necessary calculations, and the slopes vector will be given by

$$\mathbf{s}_k^{\mathrm{cl}} = \mathbf{G}_x\mathbf{x}_k + \mathbf{G}_a\mathbf{a}_{k-1} + \mathbf{n}_k. \tag{21}$$

in which $\mathbf{s}_k^{\mathrm{cl}} \in \mathbb{R}^{i}$ is the closed-loop slopes vector.

Then, Equation (16) changes to the following:

$$\mathbf{r}_k = \mathbf{E}\mathbf{s}_k^{\mathrm{cl}}, \tag{22}$$

in which $\mathbf{r}_k \in \mathbb{R}^{j}$ is the residual wavefront vector, or residual vector. Next, a estimated version of the turbulence vector is obtained from a discrete-time filter-based reconstruction, given by

$$\hat{\mathbf{x}}_k = g_k\,\mathbf{r}_k, \tag{23}$$

in which $\hat{\mathbf{x}}_k \in \mathbb{R}^{j}$ is the estimated turbulence vector and $g_k \in \mathbb{R}$ is the discrete-time filter sequence. Finally, based on (23), (17) is now rewritten as follows:

$$\mathbf{a}_k = -\mathbf{F}\hat{\mathbf{x}}_k. \tag{24}$$

Note that Equations (22)–(24) are discrete-time domain equations. In order to simplify the system analysis, these equations were mapped to the frequency domain using the unilateral $\mathcal{Z}$-transform. Thus, applying the unilateral $\mathcal{Z}$-transform in Equations (22)–(24), the actuator control vector can be defined in the frequency domain as

$$\mathcal{A}(z) = -\mathcal{G}(z)\mathbf{F}\mathbf{E}\mathcal{S}^{\mathrm{cl}}(z). \tag{25}$$

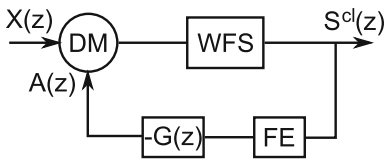

Figure 5. Block diagram of the CLC system. The DM represents the action of the deformable mirror, and WFS is the wavefront sensor. The diagram represents the actions of Equations (21) and (25).

Equation (25) is used to control an AO system by the CLC method. This method can be illustrated as a block diagram, as shown in Figure 5.

The CLC control currently being used for MCAO systems is implemented using a reconstructor computed as a regularized inverse of the interaction matrix, instead of a MVR. To differentiate these methods we will from this point on refer to them as CLC-RI, the method using regularized inverse, and CLC-MVR, the method using the MVR.

The GeMS MCAO system at the gemini south telescope (Rigaut *et al.* 2014) is an example of a CLC-RI method applied to a MCAO system. Another system running in CLC-RI is the adaptive optics facility (AOF) (Oberti *et al.* 2016). It is a laser tomography adaptive optics (LTAO) system, but its formulation is very similar to the MCAO system.

For the MVR defined in Equation (18), Equation (25) shows us a problem: the reconstruction matrix $\mathbf{E}$ is built using the turbulence covariance matrix $\mathbf{C}_{xx}$, but it is being applied to the residual phase, not to the turbulence slopes, which makes this covariance matrix not valid anymore. That is why the CLC-MVR method cannot be implemented directly, it has to be modified to operate on the slopes in open loop. A solution to this problem is the POLC method, presented in the next subsection.

3.3 *POLC method*

Ellerbroek & Vogel (2003) first proposed the POLC method: they describe it based on a hypothesis that the DM-to-WFS and turbulence-to-WFS influence matrices and the current figure of the DM are accurate and available. The classical open-loop MVR is applied to this data and the reconstructed wavefront aberrations are temporally filtered, by the use of an integrator, before they are fit to DM actuators.

Ellerbroek & Vogel (2003) and Piatrou & Gilles (2005) show the robustness of POLC method and its capability of running AO system in a closed-loop configuration. Gilles (2005) gives a theoretical proof of the stability of the POLC method, demonstrating its superior performance and superior robustness against misregistration errors compared with conventional least squares (LS) control.

The POLC method can solve the problem with the MVR involving the covariance $\mathbf{C}_{xx}$, by recreating open-loop measurements before applying the reconstruction with matrix $\mathbf{E}$. In order to apply this method, the open-loop with WFS measurements are obtained combining Equations (15) and (21)

$$\mathbf{s}_k^{\text{ol}} = \mathbf{s}_k^{\text{cl}} - \mathbf{G}_a \mathbf{a}_{k-1}, \tag{26}$$

being $\mathbf{s}_k^{\text{ol}} \in \mathbb{R}^i$ the WFS measurements for the open-loop case. Special attention here is needed: Equation (26) is actually a summation; the minus sign appears because of the actuator vector, which is already negative, as expressed in Equation (24).

In Equation (26) we consider a delay of one frame between measurements and applied input commands. Using this result to directly control the DM, as in the open-loop case, it would bring instability from noise buildup and model error of the DM response (Hardy 1998). Therefore, $\mathbf{s}_k^{\text{ol}}$ will be used only to apply the reconstruction matrix $\mathbf{E}$, with the correct turbulence covariance matrix $\mathbf{C}_{xx}$, and then, return to the residual information.

In order to define a control policy to the POLC method, one can consider first the reconstruction based on the original turbulence vector and the WFS measurements for the open-loop, as in Equation (16).

Next, using the classic definition of a residual, i.e., the difference between the exact value and the respective estimated value of a certain quantity of interest, and replacing $\mathbf{x}_k$ from Equation (16) in this definition, the residual vector can be rewritten, using Equation (26):

$$\mathbf{r}_k = \mathbf{x}_k - \hat{\mathbf{x}}_{k-1} = \mathbf{E}(\mathbf{s}_k^{\text{cl}} - \mathbf{G}_a \mathbf{a}_{k-1}) - \hat{\mathbf{x}}_{k-1}. \tag{27}$$

Applying the unilateral $\mathcal{Z}$-transform in both sides of Equation (27), in order to once again facilitate the system analysis, it results in

$$\mathcal{R}(z) = \mathbf{E}(\mathcal{S}^{\text{cl}}(z) - z^{-1}\mathbf{G}_a \mathcal{A}(z)) - z^{-1}\hat{\mathcal{X}}(z). \tag{28}$$

Now, multiplying both sides of (28) by $\mathcal{G}(z)$, it results in

$$\hat{\mathcal{X}}(z) = \mathcal{G}(z)[\mathbf{E}(\mathcal{S}^{\text{cl}}(z) - z^{-1}\mathbf{G}_a \mathcal{A}(z)) - z^{-1}\hat{\mathcal{X}}(z)]. \tag{29}$$

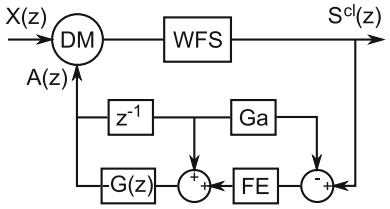

Figure 6. Block diagram of the POLC system. The DM represents the action of the deformable mirror, and WFS is the wavefront sensor. The diagram represents the actions of Equations (21) and (30).

Next, multiplying left both sides of Equation (29) by $-\mathbf{F}$, it results in:

$$\mathcal{A}(z) = -\mathcal{G}(z)[\mathbf{FE}(\mathcal{S}^{\mathrm{cl}}(z) - z^{-1}\mathbf{G}_a\mathcal{A}(z)) + z^{-1}\mathcal{A}(z)]. \tag{30}$$

This result can be represented in a block diagram form, as seen in Figure 6.

It is important to notice the difference between the CLC-MVR and POLC methods comparing Equations (25) and (30). Choosing $\mathcal{G}(z)$ as the $\mathcal{Z}$-transform of a discrete-time integrator (DTI), i.e.:

$$\mathcal{G}(z) = \frac{K}{1 - z^{-1}}, \tag{31}$$

in which $K \in \mathbb{R}^+$ is the DTI gain. We choose $\mathcal{G}(z)$ as an DTI based on following reasons: (i) it is the most common controller in AO systems; (ii) it is easy to computationally implement; (iii) it sufficiently rejects turbulence and (iv) it requires the design and tuning of a single parameter, the integrator gain K. Future work may study the use of different types of controllers.

Replacing $\mathcal{G}(z)$ in (30), one can have

$$\mathcal{A}(z) = z^{-1}\mathcal{A}(z) - K[\mathbf{FE}(\mathcal{S}^{\mathrm{cl}}(z) - z^{-1}\mathbf{G}_a\mathcal{A}(z)) + z^{-1}\mathcal{A}(z)]. \tag{32}$$

Finally, applying the inverse $\mathcal{Z}$-transform in both sides of Equation (32), the result is the following difference equation for $\mathbf{a}_k$

$$\mathbf{a}_k = (1 - K)\mathbf{a}_{k-1} - K\mathbf{FE}(\mathbf{s}_k^{\mathrm{cl}} - \mathbf{G}_a\mathbf{a}_{k-1}), \tag{33}$$

which can be defined as the control policy for the POLC method.

3.3.1 *Online application of POLC* When considering an offline application of the actual problem, the control policy is given by Equation (33). However, when it is considered an online application, the matrix product $\mathbf{F}\,\mathbf{E}$ is replaced by the matrix $\mathbf{R} \in \mathbb{R}^{\ell \times i}$, given by

$$\mathbf{R} = \mathbf{F}\,\mathbf{E}. \tag{34}$$

Mathematically speaking, Equation (34) shows not only an ordinary variable change, but it also avoids an excessive number of calculations, which is very important in computational processing. In practical applications, the matrix $\mathbf{R}$ — which is the only matrix available, instead of $\mathbf{F}$ and $\mathbf{E}$ — also brings gains in respect to processing time.

It is worth to point out that, from the point of view of control theory, $\mathbf{R}$ is the decoupling matrix of the system, as mentioned in Section 3 and, if correctly computed, it ensures the system's diagonalization.

Likewise, if the multiplication of the second subtraction term in Equation (32) is expanded, the term $\mathbf{F}\,\mathbf{E}\,\mathbf{G}_a$ arises and can be pre-calculated, which is useful from the point of view of a faster real-time processing.

4. Simulations

The results obtained in this work were done using computational simulations. To simulate an AO system we used the object-oriented MATLAB® adaptive optics (OOMAO) Toolbox (Conan & Correia 2014).

The simulation is based on a MCAO system, using three DM stack arrays, four natural guide stars, sampled by Shack–Hartmann WFS, and a grid of 3×3 science targets. The main values used in the simulation are provided in Table 1. Turbulence layers and DMs are the same quantity and are at the same altitude. This avoids some tomographic errors that are not interesting for this work.

The simulated system has misregistrations between mirror actuators and WFS to simulate an imperfect system. The misregistration is given in terms of percentage of displacement in relation to actuator spacing.

4.1 *Linear models versus nonlinear models*

In order to illustrate the performance of the HWM and its linear counterpart, SI were done to data obtained from these simulations. In Table 2, one can see the mean square error (MSE) presented in 10 randomly chosen input/output pairs of models.

One point to be highlighted is that the considered POLC system is a MIMO system, composed of n inputs by n outputs. In order to simplify the model, the MIMO system was decomposed by n SISO models (as explained in Section 2). As the number of models, n, can be high to express individually all the MSEs values, 10 of them were randomly chosen, and its mean square errors (MSE) are compared with the linear version of them.

From Table 2, one can see that the MSE for HWM is smaller than ARX models for all presented examples,

Table 1. Simulation parameters used in the experiment.

Description	Value
Telescope diameter	8 m
r_0 at 550 nm	0.12 m
Outer scale L_0	30 m
WFS wavelength	550 nm
WFS number of sub-apertures	32×32
Number of DM actuators	33×33
Target wavelength	1.654 μm
NGS magnitude	10
System frame rate	1 kHz
Angular distance between guide stars	30 arc-sec
Angular distance between target stars	30 arc-sec
Turbulence layer fractions	0.7, 0.25 and 0.05
Turbulence layer speeds	5, 10 and 20 m/s
Turbulence layer altitudes	0, 4 and 10 km
Horizontal misregistration percentage	10%
Vertical misregistration percentage	10%

Table 2. Mean square error obtained from Hamerstein–Wiener and ARX models.

Model	ARX	HWM
1	9.822×10^{-13}	1.211×10^{-15}
2	1.777×10^{-12}	4.388×10^{-20}
3	1.033×10^{-12}	1.779×10^{-15}
4	6.877×10^{-13}	1.254×10^{-17}
5	1.033×10^{-12}	1.463×10^{-15}
6	4.896×10^{-13}	6.005×10^{-17}
7	1.114×10^{-12}	4.979×10^{-17}
8	5.376×10^{-13}	4.979×10^{-17}
9	3.970×10^{-13}	1.497×10^{-17}
10	4.215×10^{-13}	2.819×10^{-17}

which is a strong suggestion that linear models are not capable to model completely a MCAO system. Furthermore, one can consider the MSE presented for the HWM is small enough to assume that the model can capture the overall system's dynamic. It is important to mention that this cases are simulated ones, and a worst signal-to-noise ratio (SNR) can increase the MSE values.

In order to analyze the stability of a MCAO system, in Section 4.2, these models will be applied with this purpose.

4.2 *Stability analysis*

The stability of a system is based on the location of its closed-loop poles (CLP) with respect to the unit radius circle (URC) in the z-plane (Ogata 1995). The location of the CLP can classify the system as: (i) stable; (ii) critically stable or (iii) unstable. This analysis can show the effects of misregistration and the open-loop gain variation based on CLP location.

Considering the problem addressed in this work, the stability of the system can be analyzed based on its response to a given disturbance; in case of an AO system, this disturbance is the atmospheric turbulence. Here, we consider that the system inputs are based on the atmospheric turbulence, and we identify the model of the system based not only on these inputs, but also in the slopes output. Furthermore, these inputs can be interpreted as a three-dimensional surface, built from the basis of $\mathbf{x}_k$, applying random coefficients for each base element and adding them.

However, in a real system, one cannot manually use the turbulence information as a system input, because we have no control over the atmospheric turbulence. In this context, one could generate an artificial turbulence with a phase screen. Nevertheless a more practical solution is to manipulate the DM, which can be done using an extra input $\mathbf{u}_k \in \mathbb{R}^{\ell}$.

In the SI method used here, we used the information received by the discrete-time integral controller as output, i.e., the information obtained after the multiplication by the control matrices. Then, for SI, the system input is $\mathbf{u}_k$; for the output, we must consider the whole system, including the action of the matrices. The output variable will be obtained in the Section 4.2.1.

The system stability analysis was done considering the following proposed hypothesis: only the dynamic part of each SISO system was investigated. In other words, the stability analysis considered that the intrinsic gain of the SISO models — represented by the 'piecewise' values in each operation point, considering the discrete-time integral controller gain — is built into each SISO model. Thus, the main component responsible for moving the poles throughout the z-plane significantly are the control actions and the proposed hypothesis becomes closer to the reality.

The SI for tuning is important in modern controllers, like predictive control, however the implementation of the controller itself is outside the scope of this work. Here we use the identification to tune integral controllers, but the real power of SI would be to use it in a more advanced controller. But this would be also outside the scope of this paper, and will be tackled as future work.

4.2.1 *System identification for stability analysis in CLC-MVR method* For the CLC-MVR system,

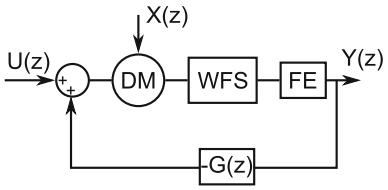

Figure 7. Block diagram for the CLC-MVR system remodeled with an extra input $\mathbf{u}_k$, which represents the disturbance for SI.

Figure 7 illustrates the mentioned extra input inclusion, which is based on the addition of an extra signal $\mathbf{u}_k$ to the mirror actuators.

It is important to mention that when input $\mathbf{u}_k$ is used, for SI purposes, the other input $\mathbf{x}_k$ is disabled. As it is not possible to control the turbulence in the SI process, the input $\mathbf{u}_k$ emulates a controllable input. In a real telescope this would mean closing the loop internally in the AO system, using an internal reference, e.g., an internal light source, to exclude the effects of atmospheric turbulence, and using the deformable mirror as the new source of simulated turbulence.

It is important to state why it was needed a nonlinear model for this identification. The system being identified is running in a closed-loop configuration, meaning that sometimes either the actuator commands or the measured slopes may become saturated. This saturation is a nonlinearity that needs to be taken into account.

Here, the controller implementation will be represented by the following difference equation:

$$\mathbf{a}_k = \mathbf{u}_k + \mathbf{a}_{k-1} - K\mathbf{FE}\mathbf{s}_k^{\mathrm{cl}}, \tag{35}$$

in which $\mathbf{u}_k$ has a zero-mean Gaussian distribution with an identity matrix for the covariance, i.e., $\mathbf{u}_k \sim \mathcal{N}(\mathbf{0}, \mathbf{I})$.

The output used for SI is given by

$$\mathbf{y}_k^{\mathrm{cl}} = \mathbf{FE}\mathbf{s}_k^{\mathrm{cl}}. \tag{36}$$

The closed-loop transfer functions obtained from the SI method have the following form

$$\mathcal{F}(z) = \frac{b_0 z^2 + b_1 z + b_2}{a_0 z^2 + a_1 z + a_2}, \tag{37}$$

in which $a_i, b_i \in \mathbb{R}$ are scalar coefficients, being $i \in \{0, 1, 2\}$. Note that Equation (37) is a proper transfer function, i.e., the degree of the numerator polynomial is equal to the denominator polynomial, with two poles and two zeros.

We implemented a simulated system and obtained data to identify a transfer function in accordance with Equation (37). In Figure 8, we have a CLP mapping in the z-plane for this system operating as CLC-MVR system. Observing this mapping, it is possible to affirm that this system is marginally stable, because there are CLP inside and on the URC, and the CLP on the URC have unit multiplicity. Therefore, a disturbance, however minor, can make the system unstable because this disturbance can cause the CLP to go out of the URC.

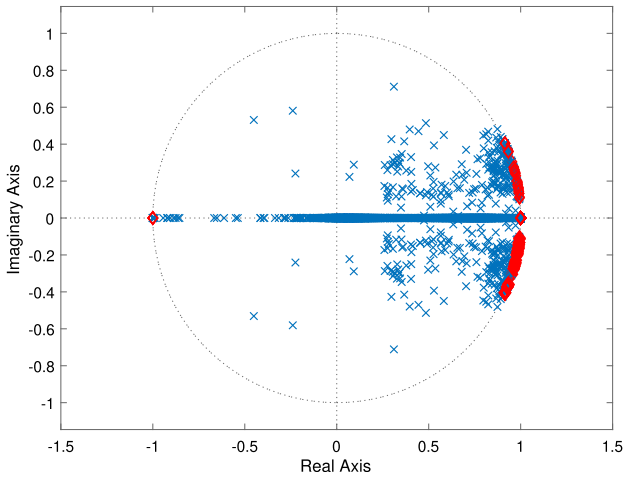

Figure 8. CLP mapping of a system working in a closed-loop configuration. The red diamonds indicate the CLP with unit multiplicity on the URC. There are 163 CLP over the URC.

Ellerbroek & Vogel (2003) and Piatrou & Gilles (2005) show theoretically that this system should be unstable. As system identification can only model what has been observed, and samples were collected from a stable closed loop system, the identified system became marginally stable, indicating possible problems with the stability in the real system, after small disturbances. In other words, in this case, the absence of poles outside URC is a limitation of the sampling step of the System Identification process, however, it is a strong suggestion of system instability, or instability reached by small perturbations.

4.2.2 *System identification for stability analysis in POLC method* In the case of POLC system, Figure 9 shows the extra signal $\mathbf{u}_k$ inclusion to the mirror actuators.

Here, the controller implementation will be represented by the following difference equation, which is a variation of Equation (33):

$$\mathbf{a}_k = \mathbf{u}_k + (1 - K)\mathbf{a}_{k-1} - K\mathbf{FE}(\mathbf{s}_k^{\mathrm{cl}} - \mathbf{G}_a\mathbf{a}_{k-1}). \tag{38}$$

Once again, $\mathbf{u}_k \sim \mathcal{N}(\mathbf{0}, \mathbf{I})$.

In the SI process, it was employed a transfer function — the linear part of the HWM — whose composition

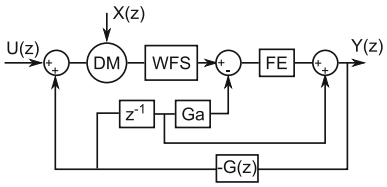

Figure 9. Block diagram for the POLC system remodeled with an extra input $\mathbf{u}_k$, which represents the disturbance for SI.

has three poles, two zeros, and no delays. The 'piece-wise linear' associated with the input of the system was composed of six linear segments. On the other hand, the 'piece-wise linear' associated with the output of system was composed of three linear segments. The parameters' estimation algorithm employed was the minimization of the prediction error method (PEM) (Isermann & Munchhof 2011).

In the POLC method, the output to be used for identification is not so clear. Then, we have to consider how the transfer function of the system is modified by the matrices multiplications, resulting in a new output $\mathbf{y}_k^{\text{polc}}$.

The transfer function of the POLC system can be obtained by analyzing the block diagram from Figure 9, resulting in

$$\mathcal{Y}_{\text{polc}}(z) = \mathbf{FE}(\mathcal{S}^{\text{cl}}(z) - \mathbf{G}_a z^{-1}\mathcal{A}(z)) + \mathbf{I}z^{-1}\mathcal{A}(z), \tag{39}$$

in which $\mathcal{S}^{\text{cl}}(z)$ is the output of the AO system, combining the actions of DM and WFS.

Considering the transfer function in (39), the new output $\mathbf{y}_k^{\text{polc}}$ can be obtained using the inverse $\mathcal{Z}$-transform in Equation (39), resulting in:

$$\mathbf{y}_k^{\text{polc}} = \mathbf{FE}(\mathbf{s}_k^{\text{cl}} - \mathbf{G}_a\mathbf{a}_{k-1}) + \mathbf{a}_{k-1}. \tag{40}$$

For a ideal system, this results in a diagonal matrix response, in which each input has a direct corresponding output, i.e., the system can be analyzed as a decentralized system with several SISO systems. With misregistration there will be elements outside the main diagonal, however since the diagonal of the matrix will have several SISO systems with the most significant open-loop gain values. Thus, the analysis of these systems brings a good approximation of the full system, preserving the computational processing time.

In Figure 10, we have the closed loop poles (CLP) from all the transfer functions obtained from the proposed POLC method, mapped in the z-plane. The CLP were obtained considering the linear part of the HWM.

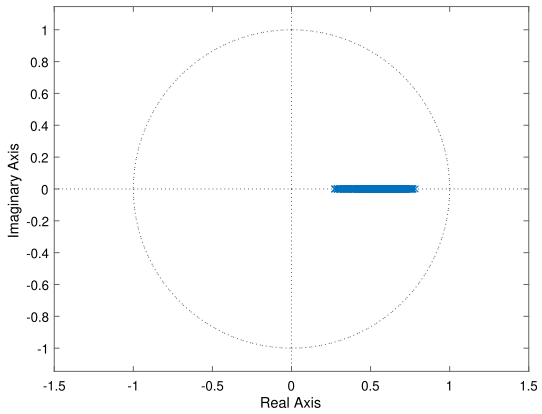

Figure 10. CLP mapping of the POLC system.

Note that there are neither CLP outside the URC, nor on the URC. This indicates that the POLC system is classified as a stable system. This stability classification was defined by the CLP with the highest magnitude value of all the CLP, which value is 0.78.

The results show what is already expected, that is, that the minimum-variance reconstructor is not stable when applied to closed loop, requiring the use of the POLC method. In the closed-loop situation, the matrix $\mathbf{E}$ is operating based on the residue, not on the measured turbulence, which invalidate the covariance matrix $\mathbf{C}_{xx}^{-1}$.

4.3 *System identification for controller design and tuning*

In this section, we propose the use of SI as an aid to the controller design and tuning. The SI itself does not need to be repeated all the time, because it identifies the dynamics within the system, that will change only when significant changes on the system are made. For example, maintenance in an optical instrument could change the optical alignment, requiring a new identification of the system.

Although the proposed models are nonlinear, they are a concatenation of the dynamics, represented by the transfer functions, and the static parts, represented by the nonlinear gain values. As the modeled system is 'piece-wise linear' it is possible to consider these linear parts only, i.e., its transfer functions, multiplied by the gain in the corresponding operation point.

In control theory, the controller gain is commonly designed and tuned based on the transfer function of the system. First, let us discuss the transfer function of an AO system submitted to a CLC-MVR. The steady state gain from each input to each output is already known in the form of the matrix $\mathbf{G}_a$. In this context,

we can consider that the main dynamic of the system is a single delay, that is caused by the WFS integration, which is much greater than any other system dynamics, e.g., the DM settling time.

It is important to note that matrix $\mathbf{G}_a$ represents only a model of the real system transformation. We will define here a transformation based on a matrix called $\mathbf{G}_a^{\text{real}}$ to denote the real system transformation, that will be close but not necessarily equal to $\mathbf{G}_a$, depending on the imperfections in modeling. Thus, the CLC-MVR system transfer function will be

$$\mathcal{T}(z) = \mathbf{G}_a^{\text{real}} z^{-1}. \tag{41}$$

However, before the signal reaches the controller, it undergoes a reconstruction based on the matrix $\mathbf{R} = \mathbf{FE}$. Then, the transfer function to be used in the CLC-MVR system case will be

$$\mathcal{T}_{\text{cl}}(z) = \mathbf{FEG}_a^{\text{real}} z^{-1}. \tag{42}$$

As mentioned before, the matrix $\mathbf{R} = \mathbf{FE}$ can be considered as a decoupling matrix, whose purpose is to decouple the various outputs. So a multivariate system can be controlled based on a combination of a several SISO systems. Indeed, the product $\mathbf{FEG}_a$ has a well-defined diagonal, close to a multiple of the identity matrix. Then, the control matrix will be a diagonal matrix, with SISO controllers occupying its main diagonal. Each controller should be designed and tuned using the corresponding transfer function.

SI can be used here to obtain a better version of these transfer functions. Misregistrations on the system and dynamic effects not considered in the theoretical model are factors that cause the transfer function obtained by means of SI methods to be more reliable.

The SI for controller design has the objective of obtaining $\mathcal{T}_{\text{cl}}(z)$ empirically, and not theoretically as was done for Equation (42), using the inputs and outputs from the point of view of the controller, disregarding the atmospheric turbulence. The turbulence is disregarded because in the case of SI for controller design we want to identify the system itself, without influence from external sources. In the case of CLC-MVR, the inputs will be the DM actuator vector a_k, and the outputs will be the product between the matrix $\mathbf{R}$ and the WFS slopes, because this is the signal vector reaching the controller

$$\mathbf{y}_k^{\text{clc}} = \mathbf{FEs}_k. \tag{43}$$

Because the system is viewed from the point of view of the controller, without it actually participating, it is effectively in open loop.

In the POLC method the theoretical transfer function is more complex. Although it can be obtained from the block diagram of the system, as viewed from the controller block in Figure 6.

Hence, in the POLC system, the transfer function will be given by

$$\mathcal{T}_{\text{polc}}(z) = \mathbf{FE}(\mathcal{T}(z) - \mathbf{G}_a z^{-1}) + \mathbf{I}z^{-1}. \tag{44}$$

In a perfect modeled system, $\mathbf{G}_a^{\text{real}} = \mathbf{G}_a$ and the value inside the parenthesis in Equation (44) would be null, but there will always be modeling errors, and the value inside the parenthesis will actually reflect these modeling errors. SI can then be used to evaluate this and obtain the real transfer function of the POLC system. The operation for identification of this type of system can be done as follows.

Considering the actuator vector $\mathbf{a}_k$, which will be the identification input, and the WFS slopes vector $\mathbf{s}_k$, the output to be used for SI in the POLC case will be

$$\mathbf{y}_k^{\text{polc}} = \mathbf{FE}(\mathbf{s}_k - \mathbf{G}_a \mathbf{a}_{k-1}) + \mathbf{a}_{k-1}. \tag{45}$$

In this case of SI for controller design, in which the system is identified in open-loop, there was no need to use nonlinear SI techniques. So the input and output parts of the HWM were not necessary, leaving only the linear central part. In the case of stability analysis in Section 4.2, it was necessary to consider the system nonlinearities because the closed-loop system may operate in a region where nonlinear effects may occur, such as saturation of the actuators or WFS.

The SI in open loop obtained by the presented method will be used next as a mathematical model of the system for controller design and tuning.

4.3.1 *Controller design and tuning* In this section, we present the method used to obtain the DTI controller gain K from (31). The tuning method is based on optimizing the integrator gain in the CLC such that the total system has the desired cutoff frequency, and that cutoff frequency is based on the turbulence statistics. Therefore, the controller gain is obtained based on the Equation (46), as follows:

$$\overline{K} = \arg\min_K \{|\omega_{\text{cutoff}}(\mathcal{G}(z)) - \bar{\omega}_{\text{cutoff}}|\} \tag{46}$$

in which $\overline{K}$ is the optimal DTI controller gain, $\omega_{\text{cutoff}}(\mathcal{G}(z))$ is the cutoff frequency of the DTI controller and $\bar{\omega}_{\text{cutoff}}$ is the desired cutoff frequency.

Figure 11 shows some Strehl ratio (S_r) $\times$ integrator gain (K) curves, based on the POLC system. The Strehl

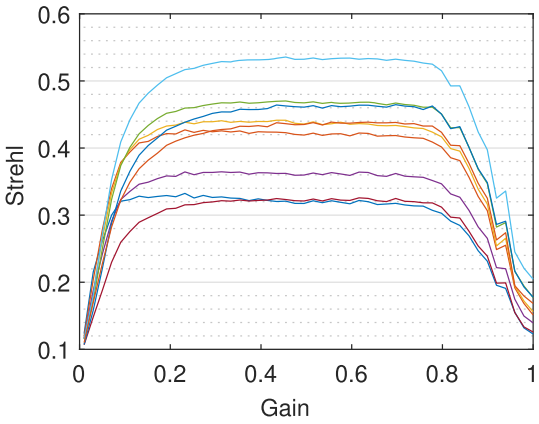

Figure 11. $S_r \times K$ curves for $1\times$ wind speed. Each line corresponds to a different star in the FoV.

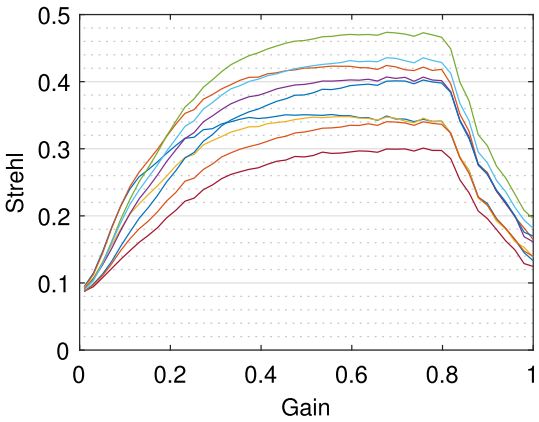

Figure 12. $S_r \times K$ curves for $3\times$ wind speed. Each line corresponds to a different star in the FoV.

ratio is a commonly used metric in AO, and represents the quality of the turbulence correction, where a unitary Strehl Ratio represents a perfect correction. These curves were obtained using the wind speed specified in Table 1. Analyzing these set of curves, it is possible to observe that the DTI controller gain values belongs to the unit interval, i.e., $K \in (0, 1]$. This occurs — for discrete-time controllers — due to gain values above 1, which leads the cutoff frequency to values above the sampling frequency.

Other interesting information obtained from the set of curves in Figure 11 is the two visible inflection points: (i) one around $K_1 = 0.1$ and (ii) other one around $K_2 = 0.8$. At the right inflection point, around $K_2 = 0.8$, the noise level is high and the chances of making the system unstable are also high, which is not desirable. Therefore, we will show in this section how to deal with the inflection point on the left.

For comparison, when the wind speed is tripled, the shape of the $S_r \times K$ curves changes, as seen in Figure 12. Note that the left inflection point moves to higher DTI controller gain values.

Considering that the transfer function of the system is known from the SI step, the control theory provides several controller design and tuning techniques in order to obtain the best controller for the system. In this paper, the design and tuning process is related to obtaining the value of the DTI controller gain value K.

A common practice in controller tuning methods is to assign desired poles — based on previously defined design requirements — in order to select the new CLP, or pseudo open loop poles (POLP), considering the system performance in terms of the frequencies of the control system loop. A DTI controller behaves as a low pass filter when it is in a closed-loop system, and the pole-placement technique could be seen equivalently to choosing a cutoff frequency.

As previously seen, the main objective in AO is to reduce, as much as possible, the effects of atmospheric turbulence, so the cutoff frequency should be higher than the frequencies present in the atmospheric turbulence. However, designing a system with a high cutoff frequency will not bring significant benefits. Actually it could impair the system performance due to higher frequencies noise.

Considering the frozen flow hypothesis (FFH), as in Poyneer *et al.* (2009), the atmospheric turbulence speed could be considered as a function of the wind speed. Normally, it is required an external measurement of the turbulence speed. In this paper, we also propose the use of the actual WFS data, next to the observation time, in order to determine the frequencies involved in the process. A time series of the WFS measurements converted to the atmospheric turbulence space basis (using the matrix $\mathbf{E}$) or to the actuator space (using the matrix $\mathbf{R}$) and obtaining the Fourier Transform of that time series, gives us the frequency behavior of the turbulence.

Here, we will analyze the turbulence in actuator space because the DTI controller in our formulation actuates there. The same analysis could be done in the turbulence space for modal control. Figure 13 shows the result for a wind with ground layer speed of 5 m/s, second layer speed of 10 m/s, and the third layer speed of 20 m/s. Figure 14 shows the same results for three times the speed values of these layers.

In Figure 13, the threshold level for the cutoff frequency, obtained empirically, corresponds to the power value of 3.7×10^{-16} dB, which corresponds to a cutoff frequency of $\omega_{\text{cutoff}} = 437$ rad/s. In Figure 14,

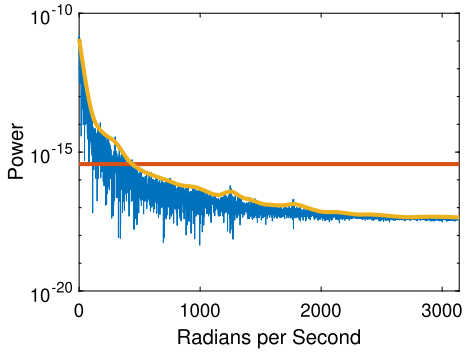

Figure 13. Frequency response of the turbulence in actuator space. The horizontal line represents the threshold level for the cutoff frequency.

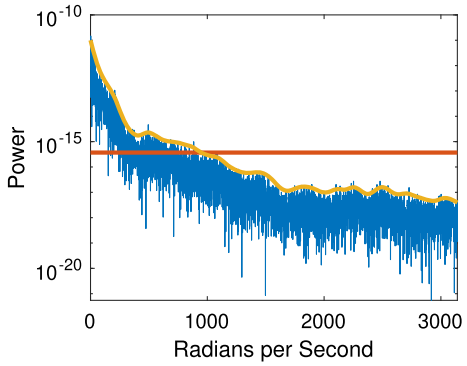

Figure 14. Frequency response of the turbulence in actuator space, with 3× wind speed. The horizontal line represents the threshold level for the cutoff frequency.

we tripled the wind speed. The threshold level for the cutoff frequency, also obtained empirically, corresponds to the same power value of 3.7×10^{-16} dB, which corresponds to a cutoff frequency of $\omega_{\text{cutoff}} = 771$ rad/s.

The obtained cutoff frequency allows the tuning of the DTI controller gain, justified by the fact that, in a closed-loop configuration, a DTI controller can be considered as a low pass filter. So, to tune this DTI controller we can use loop shaping techniques based on cutoff frequency (Åström & Hägglund 2011). These techniques normally require the transfer function of the plant to be known. Here, we also propose using the plant obtained in Section 4.3. In this work we used a simple tuning technique that searches for the DTI controller gain that results in the desired cutoff frequency, considering the resulting frequency response of the identified transfer function in closed-loop with a DTI. The search is done based on a trial and error method. More advanced design and tuning techniques may be studied and applied in future work.

Table 3. Strehl ratios (S_r) obtained for each target direction — 1× wind speed.

Target star	1	2	3	4	5	6	7	8	9
S_r	0.40	0.47	0.42	0.46	0.52	0.50	0.39	0.49	0.44

Table 4. Strehl ratios (S_r) obtained for each target direction — 3× wind speed.

Target star	1	2	3	4	5	6	7	8	9
S_r	0.35	0.44	0.38	0.41	0.50	0.48	0.34	0.46	0.41

The resulting Strehl ratio S_r for each direction is shown in Table 3. We can see that it is close to the best case scenario from Figure 11. The mean gain obtained in this tuning was $\overline{K} = 0.4012$.

In the case of triple wind speed, the resulting S_r for each direction is shown in Table 4. We can see that it is close to the best case scenario from Figure 12. The mean gain obtained in this tuning was $\overline{K} = 0.8383$.

The proposed cases illustrates the change of tuning needed when the wind speed changes, which corresponds on the change of the the disturbance frequencies as seen by the system. An identification of the system permits a tuning that filters the disturbance in the optimal position. An integral controller is very limited in this aspect and it was used here for illustration purposes. Future work will focus on the use of the identification to tune more complex controllers.

5. Conclusion

MCAO is a multivariate control problem with some special issues pertaining to the relations between discrete-time controller gains and tomography techniques. This paper approaches this problem using a mathematical modeling technique known as SI. It presents a comparison between CLC-MVR and POLC techniques, by the perspective of stability analysis of control systems.

We showed how SI can be used to analyze the stability of the system, which could help to define if the system needs to be improved or realigned. Our example of application of stability analysis showed that the POLC system is more stable that an equivalent CLC-MVR for a minimum variance reconstructor, already known in the literature, guaranteed by the location of its CLP, as seen in Figures 8 and 10.

Although the models employed in the SI process are nonlinear due to saturations, the stability analysis used are based on the 'piece-wise linear' parts of the model. In order to classify each system based on the type of stability, the position of the CLP inside the URC are considered.

Concerning the models obtained by SI it is possible to conclude that: (i) empirical models can help the designing and tuning processes of the multivariate control in MCAO systems; this is possible because the models are created based on the real implementation of the system, instead of an ideal model, which is based on some hypothesis; (ii) linear models are not capable to represent the dynamic of a MCAO system, because of the saturation in actuators and the nonlinearities of the WFS. Once the model is identified, a linear analysis is possible since AO systems are linear as long as there is no saturations and (iii) HWM approximations are close enough to represent the dynamic of the three DM.

Furthermore, it is also proposed a new methodology for design and tuning controllers for POLC method based on SI techniques. In this work we showed this proposal using one of the simplest controllers found in the discrete-time control theory, which is an integrator controller. Note that the focus of the present work was the identification itself. However future work should focus on the use of more complex controllers, as discussed in Section 3.3. Concerning the DTI proposed controller design and tuning technique, which was derived from SI, it is possible to estimate the bandwidth of each SISO system using open-loop measurements of atmospheric turbulence and consequently estimate the best cutoff frequency for each controller.

As future work the authors intend to: (i) explore other nonlinear modeling structures, e.g., volterra (separating the degrees of nonlinearities by kernel orders) or nonlinear auto-regressive moving average with eXogenous input (NARMAX) models, in order to represent the system dynamic in a more accurate way; (ii) develop analytic techniques for design and controller tuning, based on the models achieved by SI; (iii) use more advanced controllers to best make use of the possibilities leveraged by the SI.

Acknowledgements

This work was supported by the Serrapilheira Institute (grant number Serra-1709-18844) and CNPq grant number 311726/2018-6.

References

Åström K., Hägglund T. 2011, Advanced PID Control, ISA-The Instrumentation, Systems and Automation Society

Basden A. G., Jenkins D., Morris T. J., Osborn J., Townson M. J. 2019, Monthly Notices of the Royal Astronomical Society, 486, 1774

Beckers J. M. 1989, in SPIE Proceedings, Volume 1114, SPIE, Bellingham WA, p. 215

Billings S. A. 2013, Nonlinear System Identification: NARMAX Methods in the Time, Frequency, and Spatio-Temporal Domains, 1st edition, Wiley

Conan R., Correia C. 2014, Adaptive Optics Systems IV, 9148, 91486C

D'Ambrosio C., Lodi A., Martello S. 2010, Operations Research Letters, 38, 39

Ellerbroek B. L., Vogel C. R. 2003, in Astronomical Adaptive Optics Systems and Applications, Vol. 5169, International Society for Optics and Photonics (SPIE), 206

Gilles L. 2005, Applied Optics, 44, 993

Hardy J. W. 1998, Adaptive Optics for Astronomical Telescopes, Oxford University Press, New York

Isermann R., Munchhof M. 2011, Advanced Textbooks in Control and Signal Processing, Volume 1, Identification of Dynamic Systems: An Introduction with Applications, 1st edition, Springer-Verlag, Berlin, Heidelberg

Ljung L. 1999, System Identification: Theory for User, 2nd edition, Prentice-Hall, Hoboken, New Jersey

Noll R. J. 1976, Journal of the Optical Society of America, 66, 207

Oberti S., Kolb J., Le Louarn M., *et al.* 2016, Adaptive Optics Systems V, 9909, 99091U

Ogata K. 1995, Discrete-Time Control Systems, Prentice Hall

Piatrou P., Gilles L. 2005, Applied Optics, 44, 1003

Pintelon R., Schoukens J. 2012, System Identification: A Frequency Domain Approach, IEEE Press

Poyneer L., van Dam M., Véran J.-P. 2009, Journal of the Optical Society of America A, 26, 833

Rigaut F., Neichel B., Boccas M., *et al.* 2014, Monthly Notices of Royal Astronomical Society, 437, 2361

Skogestad S., Postlethwaite I. 2005, Multivariable Feedback Control: Analysis and Design, 2nd edition, John Wiley & Sons, Inc., New York, NY

Sun H., Kasdin N. J., Vanderbei R. 2018, Journal of Astronomical Telescopes, Instruments, and Systems, 4, 1

Tufa L. D., Ramasamy M., Shuhaimi M., Patwardhan S. C. 2007, in IEEE 2007 International Conference on Intelligent and Advanced Systems (ICIAS)

Wang J. Y., Markey J. K. 1978, Journal of the Optical Society of America, 68, 78

Wang L., Ellerbroek B. 2012, in Adaptive Optics Systems III, International Society for Optics and Photonics (SPIE), Volume 8447, p. 780